UNIVERSIDAD DE CANTABRIA

Departamento de Ingeniería de Comunicaciones

TESIS DOCTORAL

Cryogenic Technology in the Microwave Engineering: Application to MIC and MMIC Very Low Noise Amplifier Design

Juan Luis Cano de Diego

Santander, Mayo 2010

Chapter III
Measurement Techniques for Cryogenics

The design of any circuit starts with the modelling of its different components and finishes with the characterization of the circuit itself. Both for taking measurements, from where the required models are extracted, and for characterizing the final design, different measurements have to be performed. In the case of low noise amplifiers Scattering parameters (S-parameters) and noise measurements are usually enough for modelling and final characterization.

In cryogenics these measurements are even more challenging than at room temperature. For the S-parameters measurement the desired calibration planes are not directly accessible and therefore some modifications to the classical measurement techniques have to be applied. These modifications usually compromise the measurement accuracy. For the noise, not only the calibration planes are not accessible but also the noise source powers involved in the RT techniques are large compared with the measured noise values, which affects noise accuracy.

This chapter gives an overview of some calibration methods to measure cryogenic S-parameters focusing in a technique to avoid drift errors as well as systematic errors in the RF range. Then, the cold-attenuator technique, which is one of the most widespread methods for measuring noise in cryogenics, is explained in detail. Moreover, a comprehensive study of the uncertainty in this technique using Monte-Carlo analysis is presented. Finally, it is shown a new design of a chip attenuator that improves accuracy in noise measurements with the cold-attenuator technique.

3.1. Overview of Calibration Techniques for Cryogenic S-Parameters Measurements

The calibration is a process through which different precisely known devices, called *standards*, are measured using a network analyzer in order to obtain the differences between measured and actual values. From these measurements, a set of parameters, called *error terms*, describing the test set are calculated, and the measurement reference plane is moved to the DUT ports.

The above mentioned error terms characterize the systematic errors introduced by the network analyzer and the different hardware used to connect this equipment to the DUT (cables, connectors, adapters…). These systematic errors are time invariant and therefore can be characterized and eliminated through proper calibration [3.1]. As well as these, random errors and drift errors may be present during the measurements; the firsts are randomly time variant so they can not be eliminated, while the later are produced by performance variations of the different components once the calibration has been made. These variations are mainly produced by temperature changes and can be eliminated with successive calibrations.

At room temperature (T = 296 K) several calibration techniques can be applied to eliminate systematic errors [3.2]-[3.4]. The connection of the different standards at the desired calibration plane is straightforward and it is not time consuming, which avoids the appearance of drift errors.

At cryogenic temperature the DUT is enclosed by the Dewar so that its ports are not directly accessible. Therefore, calibration techniques applied at room temperature need to be conveniently modified. At this point it is needed to define the concept of *thermal cycle*, which is the period of time that includes a cryostat cooling down to the test temperature, a measurement, and a cryostat heating up to room temperature. A thermal cycle usually takes several hours, ranging from five hours to one day depending on the available cryogenic system. According with this definition, the different measurement techniques can be divided into two main groups: those which need only one thermal cycle for the calibration and measurement, and those which need one thermal cycle for each standard characterization during calibration and one last thermal cycle for the final measurement. From the previous classification it is clear that measurement techniques included in the second group may be affected by drift errors that need to be removed for precise calibration.

3.1.1. Measurement techniques involving one thermal cycle

In these techniques all the standards are introduced at the same time together with de DUT in the Dewar. Once the cryostat is cooled, the calibration is performed and the

measurement is taken. The complete calibration process is carried out just before the measurement, thus avoiding the appearance of drift errors. Any of the calibration techniques developed for room temperature can be used with these measurements just introducing the suitable number of standards. The problem arises with the method followed to exchange from one standard to other at the desired calibration plane. Depending on the selected method the measurement accuracy can be seriously affected.

For components or devices (not connectorized) the characterization can be made fast and accurate if a cryogenic probe station is available [3.5]-[3.7]. In this case a calibration substrate including all the standards is cooled close to the DUT and the measurement is made in the same way as at room temperature. Modification of standards electrical characteristics with temperature may affect the measurement precision.

If a cryogenic probe station is not available or the components and systems are connectorized then different electrical paths are used for each element. The differences between paths, which are assumed to be equal, produce a degradation of measurement accuracy, limiting the maximum frequency range. To change between these different paths it is necessary a switching method either inside or outside the Dewar.

An electromechanical switch can be used inside of the Dewar to exchange between the different standards and the DUT. The advantage of this option is that only one RF feedthrough is needed for all the elements and therefore the differences between paths are reduced. The main drawback is that a switch covering the full band and working at cryogenics with small or negligible differences between its ways may be very difficult or impossible to find. A sketch of a calibration and measurement using this procedure is shown in Fig. 3.1.

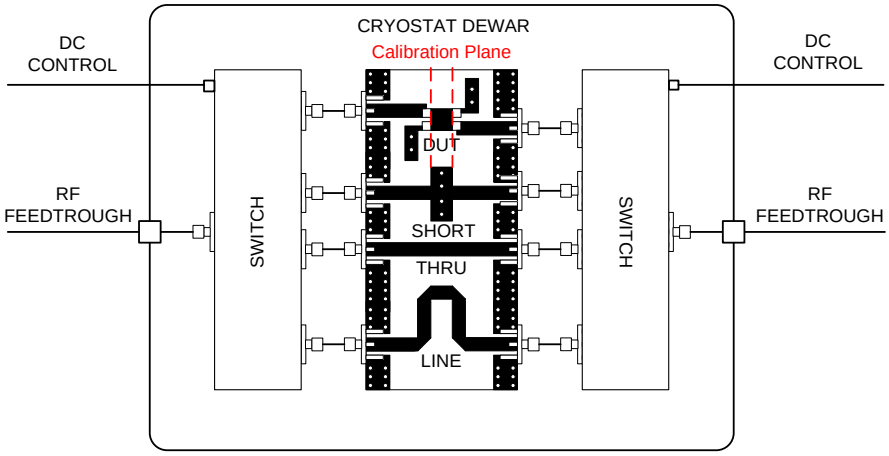

Figure 3.1. Example of calibration and measurement in one thermal cycle using switches inside the Dewar. A Thru-Reflect-Line (TRL) calibration technique is applied in this example through a home-made TRL test-fixture designed for non-insertable devices. The calibration plane is moved from network analyzer to DUT ports.

An alternative to the previous method is to use a feedthrough for each element in the cryostat [3.8]. The switch between different feedthroughs can be made manually outside the Dewar. The advantage of this technique is the absence of switches working at cryogenic temperatures which eliminates a great source of inaccuracy; on the other hand, the main drawback of this method is the need of electrically similar feedthroughs and connectors. The more different they are the lower maximum frequency they can be used. Figure 3.2 shows this alternative technique.

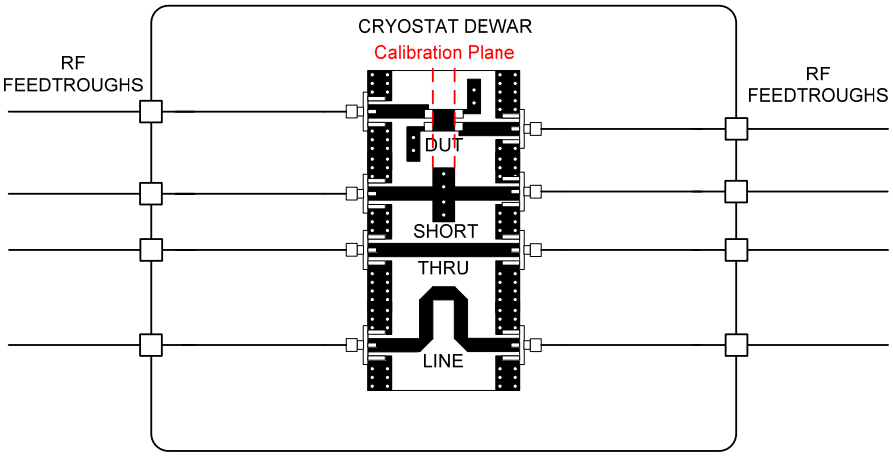

Fig. 3.2. Example of calibration and measurement in one thermal cycle using different feedthroughs for the standards and DUT. A Thru-Reflect-Line (TRL) calibration technique is applied in this example through a home-made TRL test-fixture designed for non-insertable devices. The calibration plane is moved from network analyzer to DUT ports.

3.1.2. Measurement techniques involving several thermal cycles

In these techniques more than one thermal cycle is necessary depending on the calibration method and the selected strategy. The main advantage of these techniques is that all the elements during the calibration and measurement have the same, or almost, electrical path; but, as a consequence of the very time consuming calibration procedure, drift errors may be present in the measurement.

Following with the example presented in Fig. 3.2, a measurement applying the Thru-Reflect-Line (TRL) calibration could be carried out in four thermal cycles if only two feedthroughs are used. In each thermal cycle one standard is connected to the feedthroughs while the other elements are left open. Between thermal cycles, the element to be measured must be changed manually. In this technique different connectors are used for each standard and DUT. Since these connectors are considered to be electrically equal during the calibration then the measurement accuracy is affected.

To overcome the problem of different connectors in non-insertable devices special test-fixtures can be developed [3.9]. This technique improves calibration accuracy and can be used at higher frequencies than the other techniques. The problem is to design a test-fixture readily configurable for different devices and standards that works properly

at cryogenic temperatures with a minimum size. There are some commercial alternatives for room temperature test-fixtures [3.10] but they are too big to be installed in the Dewar and their performances under cryogenic temperatures have not been checked.

Finally, a hybrid technique is applied in [3.11] to measure S-parameters of a connectorized system. In this technique the main calibration is made at room temperature at the desired reference plane using an electronic calibration kit. Then it is supposed that small variations are produced upon cooling and some modifications are applied to the first calibration to take into consideration these variations. These variations are obtained from the measurement of different standards in different thermal cycles. The advantage of this method is that the characterization of the above mentioned variations are performed once for the available setup and only the room temperature calibration is needed for the subsequent measurements. The drawback of this technique is that it is only advantageous if the setup in the Dewar is always the same, i.e. the reference is always set at the same plane, otherwise this technique has the same advantages and disadvantages than the others presented in this section.

3.1.3. Accurate Thru-Reflect-Line calibration avoiding drift errors

Excluding on-wafer measurements with a cryogenic probe station, among the measurement techniques presented in previous sections those which need several thermal cycles are more accurate since they use the same electrical path for all the elements.

The TRL calibration is one of the most accurate techniques within the room temperature calibration methods using a minimum number of standards: one Thru, one Reflect (either Short or Open) and a Line ($\lambda/4$ longer than Thru standard at central frequency). On the other hand, it has a limited bandwidth (frequency span/start frequency ratio of 8:1) that can be extended using additional Line standards [3.12].

Since the TRL calibration uses minimum number of standards the calibration process is faster than other techniques such us Short-Open-Load-Thru (SOLT) which requires one thermal cycle more. Therefore the TRL method has been selected in this thesis to be adapted to cryogenic measurements. The basic setup for applying TRL calibration is shown in Fig. 3.3.

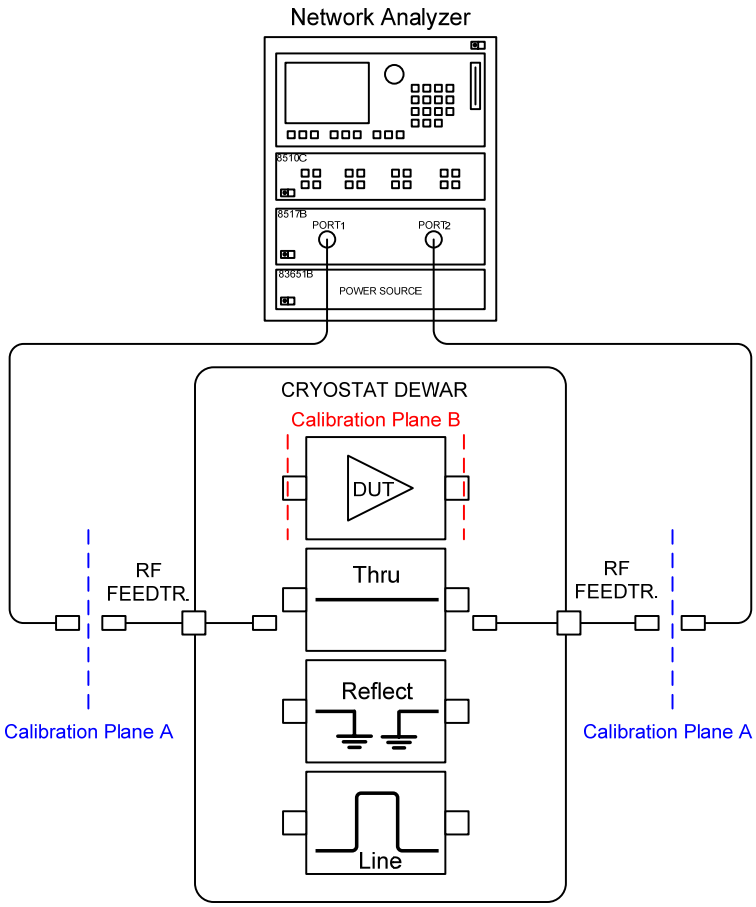

Fig. 3.3. Measurement setup applying TRL calibration at cryogenic temperature.

In the general calibration procedure at cryogenics the network analyzer remains uncalibrated until all the standards are measured which usually takes many hours or even days. Moreover, once the network analyzer is calibrated, the DUT measurement is delayed one additional thermal cycle. If the measurement equipment is prone to vary its performance with time then drift errors will be present in the final measurement.

As stated in Section 3.1, drift errors can be eliminated with successive calibrations, therefore a modification of the general calibration procedure to enable calibration of the network analyzer before each measurement is proposed in this thesis. The main idea behind this modification is to perform the calibration calculations (at reference plane B in Fig. 3.3) using a computer, while the network analyzer is used only to obtain the different measurements during the time consuming calibration. Since it is not necessary to keep the standards measurements in the analyzer memory during the calibration, then this equipment can be calibrated (at reference plane A in Fig. 3.3) before each standard is measured, thus eliminating its drift errors. Once the systematic and drift errors of the network analyzer have been eliminated, the DUT S-parameters at reference plane B need to be obtained using the different measurements taken at reference plane A. The calculations to eliminate de systematic errors in the setup between reference planes A and B are presented in the following subsection.

3.1.3.1. Theoretic background of TRL calibration

In general, systematic errors associated with a two-port system can be characterized with a set of twelve error terms [3.13].

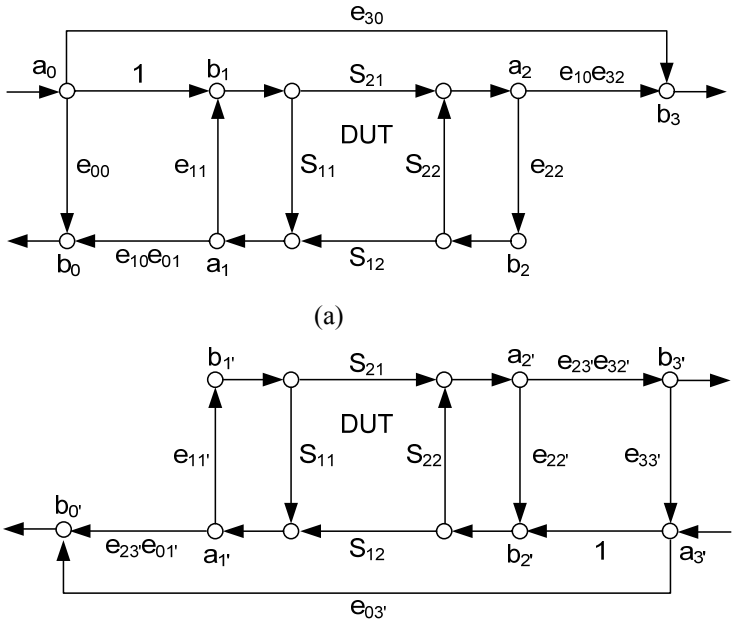

Fig. 3.4. Two-port 12-term error model; (a) 6-terms forward, (b) 6-terms reverse.

The meaning of the different terms is the following:

- e_{00}: Forward directivity
- e_{11}: Port-1 match in the forward direction
- e_{22}: Port-2 match in the forward direction
- $e_{10}e_{01}$: Forward reflection tracking
- $e_{10}e_{32}$: Forward transmission tracking
- e_{30}: Forward isolation
- e_{33}': Reverse directivity
- e_{22}': Port-2 match in the reverse direction
- e_{11}': Port-1 match in the reverse direction
- $e_{32}'e_{23}'$: Reverse reflection tracking
- $e_{23}'e_{10}'$: Reverse transmission tracking
- e_{03}': Reverse isolation

In the TRL technique the calculation of these terms starts with the separation of the measurement system in two different parts containing the terms at the input and output of the DUT. In order to do this, it is necessary to eliminate the isolation error terms [3.13]. The measurement of these terms is carried out through the use of matched loads at both ports and measuring both parameters S_{21} and S_{12}, thus:

$$e_{30} = S_{21}^{m} \tag{3.1}$$

$$e_{03}^{'} = S_{12}^{m} \tag{3.2}$$

Where superscript *m* denotes that the parameters are *measured*. If the insertion loss of the DUT is not high (same order of the test-fixture or equipment isolation), then these terms can be estimated as zero and therefore they can be omitted in the calibration process [3.14]. After separating the error set into two blocks the new flow graph representing the system is as shown in Fig. 3.5.

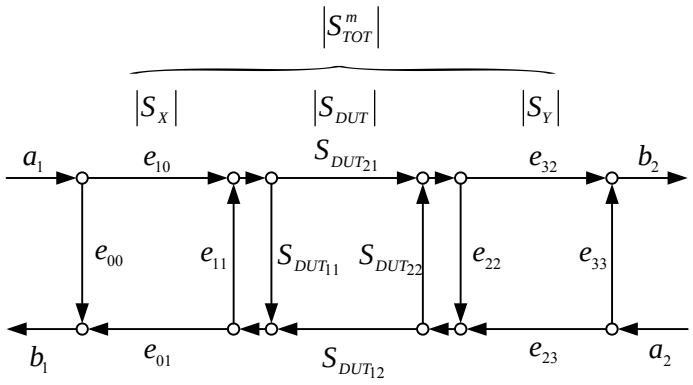

Fig. 3.5. 8-term error model.

Now the problem is reduced to find eight error terms. This is the model associated to old network analyzers, such as 8720C from Hewlett-Packard, which can not distinguish between the internal matching of port 1 and port 2, and therefore they assume that the impedance of the internal switch is the same in both directions [3.15]. Newer network analyzers, such as model 8510C from Hewlett-Packard, can perform measurements to eliminate the errors introduced by the switch at its different states.

According with the calibration procedure proposed in this thesis, once the standards and the DUT have been measured at calibration plane A there is a set of four S-parameter files, which are conveniently manipulated to obtain first the eight error terms in Fig. 3.5 and finally the DUT S-parameters at calibration plane B. These error terms represent the test-fixture between calibration planes A and B.

The DUT S-parameters at calibration plane B are obtained with equations (3.3)-(3.6).

$$S_{DUT11} = \frac{e_{22}S_{TOT12}^{m}S_{TOT21}^{m} + \left(e_{00} - S_{TOT11}^{m}\right)\left(e_{22}S_{TOT22}^{m} - \Delta S_Y\right)}{D} \tag{3.3}$$

$$S_{DUT22} = \frac{e_{11}S_{TOT12}^{m}S_{TOT21}^{m} + \left(e_{33} - S_{TOT22}^{m}\right)\left(e_{11}S_{TOT11}^{m} - \Delta S_X\right)}{D} \tag{3.4}$$

$$S_{DUT12} = \frac{-e_{10}e_{32}S^{m}_{TOT12}}{D} \tag{3.5}$$

$$S_{DUT21} = \frac{-e_{01}e_{23}S^{m}_{TOT21}}{D} \tag{3.6}$$

Where,

$$D = e_{11}e_{22}S^{m}_{TOT12}S^{m}_{TOT21} - \left(e_{11}S^{m}_{TOT11} - \Delta S_X\right)\left(e_{22}S^{m}_{TOT22} - \Delta S_Y\right) \tag{3.7}$$

$$\Delta S_X = e_{00}e_{11} - e_{01}e_{10} \tag{3.8}$$

$$\Delta S_Y = e_{22}e_{33} - e_{23}e_{32} \tag{3.9}$$

A comprehensive derivation of the previous expressions can be found in Annex II. These calculations are based in the information given in [3.3], [3.13], [3.16] and [3.17].

3.1.3.2. Experimental verification of the proposed technique

The experimental verification of the technique presented in the previous section is carried out at room temperature since a suitable DUT cryogenic measurement is not available to compare with. However the calibration procedure is carried out in the same way as it was for a cryogenic measurement.

A transistor, model ATF-551M4 from Avago Technologies, is mounted in a suitable test-fixture designed for measuring it applying the TRL calibration technique in the 0.4 to 3.2 GHz band (8:1). This test-fixture, shown in Fig. 3.6a, also includes the Thru, Reflect (short-circuit) and Line standards. The test-fixture emulates the measurement setup of Fig. 3.3 where the calibration plane A would be the coaxial connectors reference plane in Fig. 3.6a, and calibration plane B would be the transistor reference plane. Hence, the contribution of the different coaxial connectors and the network analyzer drift errors is corrected with this technique in this case.

First, the network analyzer is calibrated at calibration plane A (coaxial calibration – SOLT) and then one of the standards is measured from this calibration plane. Afterwards, the analyzer is returned to its original state (PRESET) to simulate the loss of calibration accuracy produced by time consuming measurements (drift errors). This procedure is repeated for the other standards and for the transistor biased at the desired bias point, in this case V_{ds} = 2V and I_{ds} = 10 mA. Second, these four measurement files are introduced in the developed software to calculate the transistor S-parameters at calibration plane B (3.3)-(3.6). Finally, the same transistor is measured once again but in this case using the normal TRL technique at calibration plane B to compare with the calculated result. This comparison is presented in Fig. 3.6 showing almost identical curves between the calculated (red curves) and measured (blue curves) S-parameters.

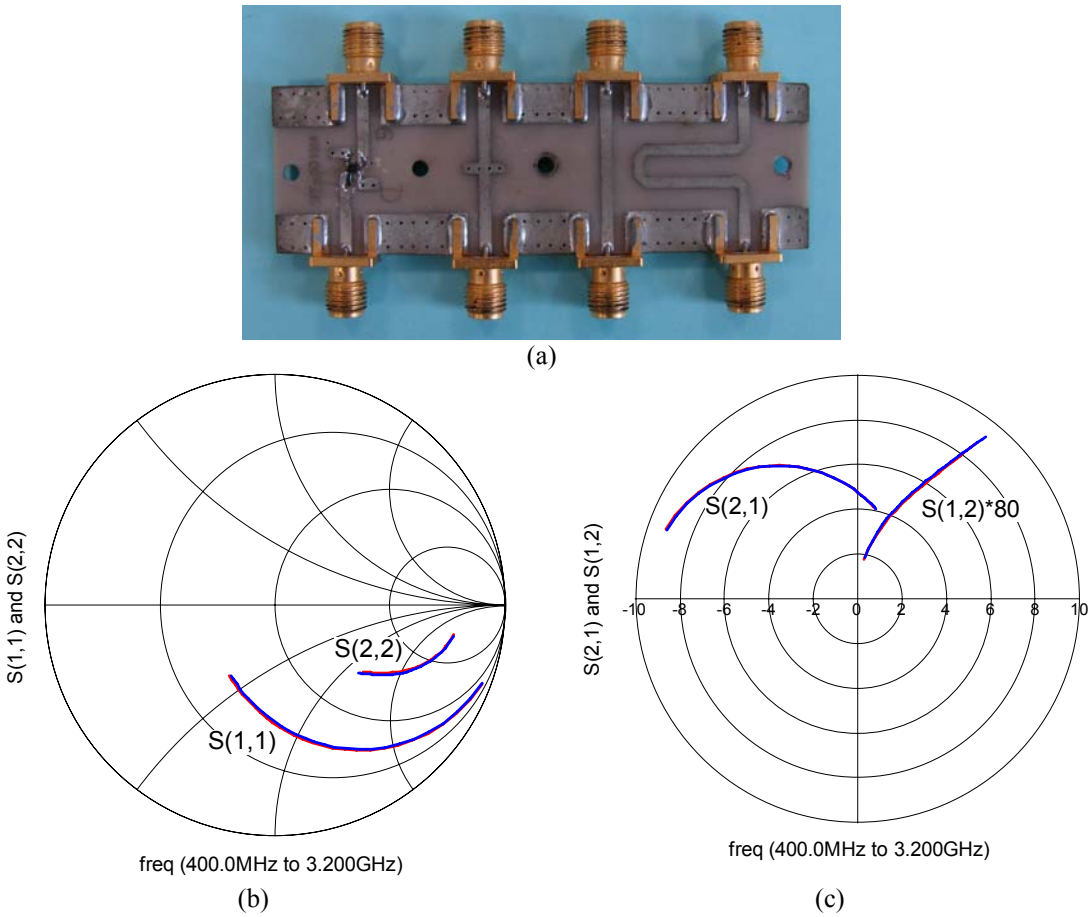

Fig. 3.6. Comparison of the TRL calibration technique between the normal procedure not suitable for cryogenic application (blue) and the proposed procedure adapted for cryogenic application (red); (a) TRL test-fixture; (b) measured and calculated S_{11} and S_{22}; (c) measured and calculated S_{21} and S_{12}.

3.2. Noise Measurement at Cryogenics: Cold-Attenuator Technique

3.2.1. Introduction to the noise measurement

The noise measurement is probably the most important measurement for microwave engineers working at cryogenics since the main objective behind cooling the systems is the reduction of its thermal noise.

Most of the noise measurement techniques, both at room and cryogenic temperatures, are based on the noise linearity of two-port linear systems. The noise power at the system output is linearly dependant on the noise at the input [3.22].

If one point and the slope, or two points, of the straight line that defines the linear system are known, then the noise power at the output, without noise at the input, i.e. the noise added by the DUT, N_a, can be obtained. From this value it is easy to calculate the *noise factor*, F, or the *effective input noise temperature*, T_e, through (3.10) and (3.11). Therefore, it would be enough a noise source providing two noise powers (T_c and T_h), and the measurement of the output powers, to be able to trace the straight line as presented in Fig. 3.7. This technique is known as *Y-Factor* method.

$$F = \frac{N_a + kT_0BG}{kT_0BG} \tag{3.10}$$

$$T_e = \frac{N_a}{kGB} \tag{3.11}$$

Where k is the Boltzmann's constant ($k = 1.38 \cdot 10^{-23}$ J/K), B is the bandwidth, and T_0 is an IEEE standard temperature defined as $T_0 = 290$ K.

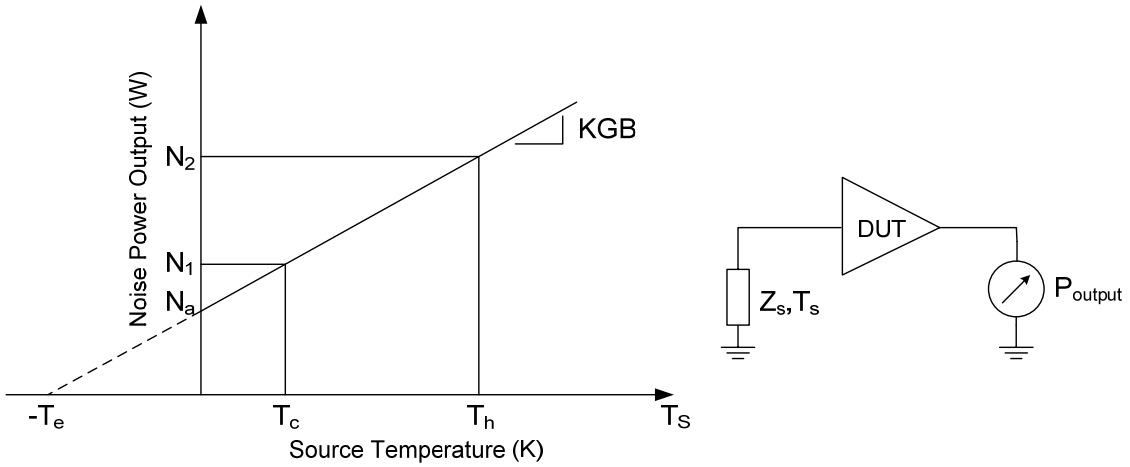

Fig. 3.7. Relationship between source temperature and noise output power in linear two-port systems. If the source temperature is zero then the output power is the noise added by the system, N_a, which is related with its effective input noise temperature, T_e.

The effective input noise temperature is a parameter much more useful for low noise devices such as found in cryogenic applications. T_e is preferred for low noise devices because it is a more sensitive indicator when N_a is small. From Fig. 3.7 a more convenient equation for calculating T_e can be obtained (3.12). This equation shows that T_e has not a reference temperature and uses the Y-Factor, which is the ratio of the output noise powers measured at the receiver when two different input noise powers are presented to the DUT.

$$T_e = \frac{T_h - YT_c}{Y - 1} \tag{3.12}$$

To obtain a precise noise measurement it is advisable that the measured value of T_e to be between T_c and T_h or, at least, to be as close to T_c as possible. In cryogenics T_e has very low values compared with the noise powers delivered for common noise sources. Due to the random nature of these signals a small error in their measured values in the receiver may produce large errors in the calculation of T_e. To overcome this problem there are several techniques developed in cryogenics to reduce the noise powers at the input of the DUT. Some of them use alternative noise sources providing adequate power values, while others try to reduce the noise powers arriving to the DUT

introducing some element with high insertion loss before the DUT. All these techniques, briefly described in [3.23], are commented in next section for completeness.

3.2.2. Overview of noise measurement techniques in cryogenics

3.2.2.1. Hot and cold loads

In this technique, two independent loads are placed outside the cryostat providing suitable input noise powers. These two loads are connected to the input line through a switch avoiding the need of connect and disconnect alternatively the loads and thus speeding up the process. A sketch of this technique is shown in Fig. 3.8.

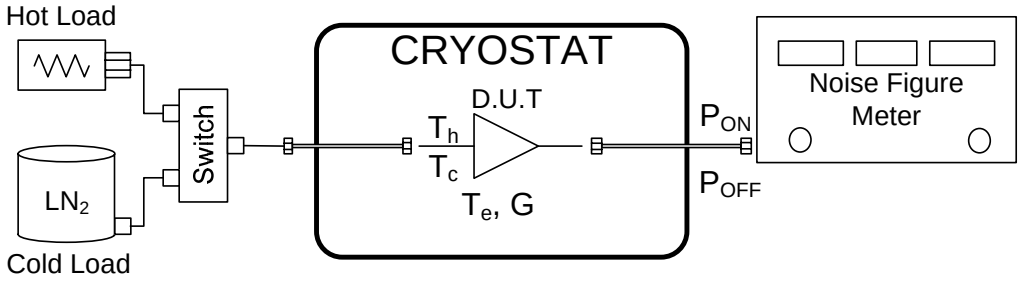

Fig. 3.8. Diagram of the hot and cold loads noise measurement technique.

Usually, the hot load is a resistor at room temperature which provides a T_h of around 300 K while the cold load is a resistor immersed in liquid nitrogen (LN_2) which produces a T_c around 77 K. This technique has some problems related with its accuracy:

- The accuracy of noise measurement is greatly dependent on the difference between the impedances presented by the loads to the DUT, which usually differ significantly from each other.
- Long-term repeatability of insertion loss and impedance match of the switch is crucial for accurate results.
- Commercial cold loads are bandwidth limited and custom equipment needs to be developed for high frequency measurements.
- Even though the noise measurement can be automatized the test speed is slow hindering the optimization process when several measurements are required.
- Finally, the noise powers at DUT input may be still far from the measured T_e value, leading to inaccuracy problems.

3.2.2.2. Noise figure meter with noise diode

This is the typical technique used for noise measurements at room temperature. In this method a solid-state noise diode is used as a noise source producing two different noise powers when it is switched from one state to other. A block diagram of this setup is shown in Fig. 3.9.

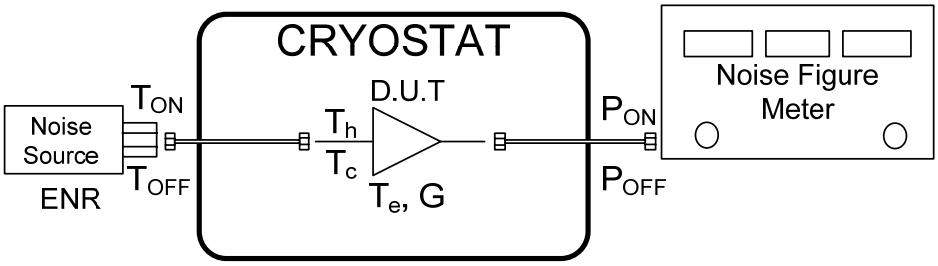

Fig. 3.9. Diagram of the noise measurement technique with noise figure meter and noise diode.

The noise temperatures at the noise source output are very different in this technique ranging from around 300 K, when the diode is in its OFF state, and thousands of kelvins, depending on the diode Excess Noise Ratio (ENR), when the diode is in ON state. Therefore, this method is suitable for devices with effective input noise temperatures included in the previous range. But, at cryogenics this method presents two main problems:

- The effective input noise temperature of cryogenic amplifiers is well below 50 K in the frequency range where these noise diodes are used and then the error produced by this approach is noticeable.
- The noise source output impedance changes significantly from one state to other producing an important ripple in the noise measurement. Moreover, the DUT's input noise temperature is also raised due to the impedance changes. Noise sources with low ENR are preferable for this technique since they are made placing a suitable attenuator at the source output, thus reducing the ENR value and the differences between output reflection coefficients.

3.2.2.3. Hot and cold load

This technique should not be confused with the first one presented in Section 3.2.2.1. Now there is only one load placed at the DUT's input inside of the Dewar. This load is cooled by the cryostat and heated up with a resistor attached to it in order to produce the two different noise powers needed for the Y-Factor method. The sketch of this technique is shown in Fig. 3.10.

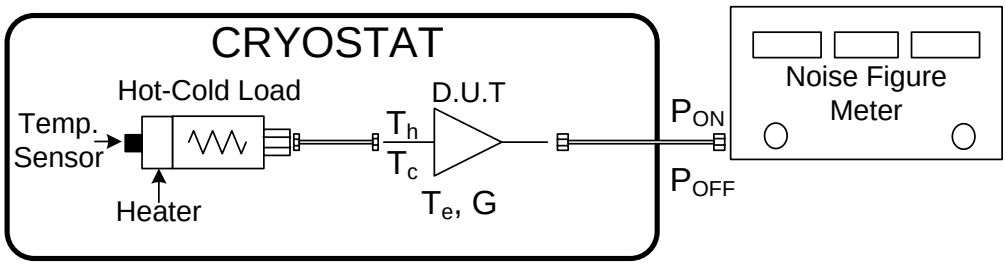

Fig. 3.10. Diagram of the hot and cold load noise measurement technique.

This technique overcomes many of the drawbacks of previous methods. First, the differences between load reflection coefficients in both states, cold and hot, are likely small which reduces the uncertainty in noise measurements; and second, when the heater is OFF the load is at the same physical temperature as the DUT, thus producing a T_c value close to the measured T_e value. On the other hand, two serious problems still remain in this technique:

- The cooling and heating processes are very slow and therefore the test speed is reduced considerably, making this technique inadvisable for broadband measurements if another method is available.
- In order to apply this technique special care must be taken to avoid DUT to be heated when the heater is ON, otherwise the noise results will be affected by this temperature increment. A good thermal isolation between the load and the DUT could be very difficult to achieve.

3.2.2.4. Cold sky and ambient aperture load

In this technique a calibrated test feedhorn, with a very low side-lobe pattern to minimize ambient noise pickup from the ground, is placed at room temperature at the input of the DUT. The cold temperature is just the sky temperature which has a value of a few kelvins, while the hot temperature is accomplished through the use of an aperture load at ambient temperature. A radiometer is used to measure the power ratio between the sky and the ambient aperture load as shown in Fig. 3.11.

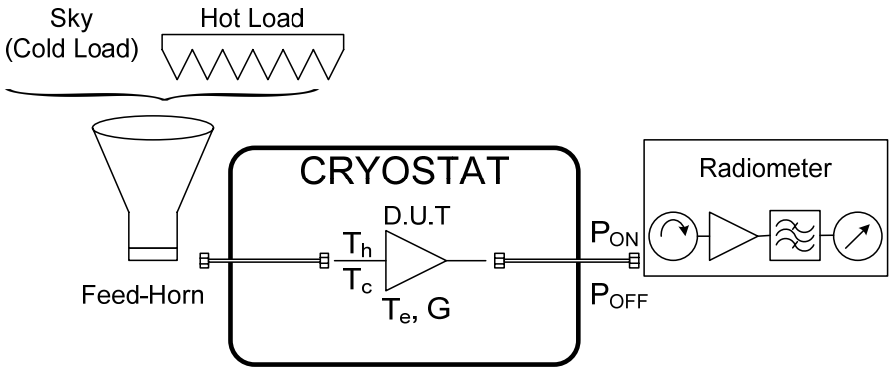

Fig. 3.11. Diagram of the cold sky and ambient load noise measurement technique.

This method has the advantage of achieving high precision for frequencies below the millimeter-wave range since the atmospheric weather has small effects in the reference sky temperature. Furthermore, the noise measurement is made with the DUT installed in an antenna, which reproduces its final application and therefore the measurement conditions are more realistic. On the other hand, this technique has some drawbacks:

- The calibrated feed-horn may be difficult to design depending on the frequency and bandwidth.
- The measurement setup needs to be placed in a suitable location with stable and characterized atmospheric conditions. The noise measurement accuracy is greatly affected by the cold temperature reference. Radio observatories are usually the only place where this technique is applied.
- The test speed is low due to manual switching between loads.

3.2.2.5. Cold-attenuator technique

In Section 3.2.2.2 it was commented that the use of low ENR noise sources was advisable due to the reduction of differences between the output reflection coefficients in both source states. The decrease of ENR in a noise source is achieved introducing a suitable attenuator after the noise diode and thus the differences between the above mentioned impedances are reduced twice the attenuation value [3.24].

The cold-attenuator technique is a modification of this method in the way that an attenuator is placed and cooled before the DUT, inside of the Dewar as shown in Fig. 3.12. With this approach, as well as an improvement in the reflection coefficients variation, there are three more important advantages:

- The noise powers are attenuated before the DUT, thus providing suitable power values for the Y-Factor method in a cryogenic environment. When the noise source is OFF then the T_c value is the physical temperature of the attenuator plus few kelvin resulting from the T_{OFF} (T_{OFF} ~ 300 K) value attenuated by the cold-attenuator; when the noise source is ON the high T_{ON} value (typically T_{ON} > 9000 K) is attenuated obtaining a suitable T_h value around 100 K or less.
- The temperature and insertion loss profile in the input line is important for accurate noise measurements. In this technique the insertion loss of the input line can be made negligible regarding the attenuator insertion loss and therefore this method is less sensitive to errors in the temperature and insertion loss characterization of the input line.
- Finally, no mechanical switches are needed and thus the test speed is improved, enabling fast and broadband noise measurements.

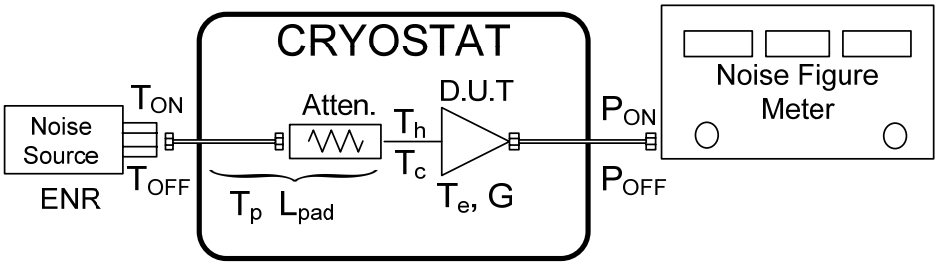

Fig. 3.12. Diagram of the cold-attenuator noise measurement technique.

Assuming that the input line has a constant temperature distribution and a constant propagation loss the temperatures at the DUT input can be calculated with (3.13) [3.25]. If the insertion loss of the input line is not negligible compared with the attenuator then the previous simplification may lead to noticeable errors and then a linear temperature distribution has to be considered in this input line. Expressions for calculating the input temperatures in this last case can be also found in [3.25].

$$T_{h,c} = \frac{T_{ON,OFF}}{L_{pad}} + T_p\left(1 - \frac{1}{L_{pad}}\right) \tag{3.13}$$

Where T_p is the physical temperature of the attenuator and L_{pad} the total insertion loss of the input line including the attenuator. If the input path is fully characterized in the measurement band then the calculation of the input temperatures is straightforward and the calculation of T_e is simple using (3.12).

There are many factors which influence the accuracy of the noise measurement with the cold-attenuator technique, but in many cases the error in the value of the cold reference becomes dominant [3.24], [3.26]. A high value of the insertion loss in the attenuator will help in providing a well defined cold reference; however this value should be kept within adequate limits in order to improve the noise measurement accuracy. It is clear that small attenuation values should not be used in order to avoid problems commented previously. On the other hand, large attenuation values produce small differences between the hot and cold temperatures at the DUT input. The random nature of noise signals produce fluctuations in the power measured by the noise figure meter. These small fluctuations may generate a large measurement error when calculating the Y-Factor if the differences between hot and cold temperatures are small [3.22].

Therefore, there should be an optimum value of the insertion loss of the attenuator which may be dependent on the details of the measurement setup. In the following calculation, a simple setup is considered where only the fluctuations in received noise powers, due to limited receiver bandwidth and integration time, are taken into account.

From (3.12), to obtain the optimum insertion loss for the attenuator it is needed to calculate the minimum T_e uncertainty due to the uncertainty in Y, produced by the fluctuations in noise power measurements. Equation (3.14) gives the standard deviation of T_e, ΔT_e, in terms of standard deviation of Y, ΔY.

$$\Delta T_e = \frac{\partial T_e}{\partial Y} \Delta Y \tag{3.14}$$

For this simple approach, it can be considered that Y is function of two uncorrelated random variables, noise powers P_{ON} and P_{OFF}, and therefore ΔY can be calculated from (3.15).

$$\frac{\Delta Y}{Y} = \sqrt{\left(\frac{\Delta P_{ON}}{P_{ON}}\right)^2 + \left(\frac{\Delta P_{OFF}}{P_{OFF}}\right)^2} \tag{3.15}$$

Fluctuations in the measured powers are dependent on the noise figure meter bandwidth, B, and integration time, τ, as stated in (3.16).

$$\Delta P_{ON,OFF} = \frac{P_{ON,OFF}}{\sqrt{B \cdot \tau}} = \frac{(T_{h,c} + T_e) \cdot kGB}{\sqrt{B \cdot \tau}} \tag{3.16}$$

Where k is the Boltzmann's constant and G the DUT transducer gain. Introducing (3.16) and (3.15) in (3.14) the standard deviation of T_e is obtained as a function of T_h and T_c (3.17), which are dependent on the attenuator insertion loss (3.13).

$$\Delta T_e = \sqrt{\frac{2}{B \cdot \tau}} \frac{(T_h + T_e)(T_c + T_e)}{(T_h - T_c)} \tag{3.17}$$

Combining (3.17) and (3.13) the optimum value for the attenuator insertion loss, for a given setup, can be obtained. In Fig. 3.13, ΔT_e as a function of total path attenuation is plotted for the following setup: B = 4 MHz, τ = 1 sec, T_p = 15 K, T_e = 20 K and T_{OFF} = 296 K.

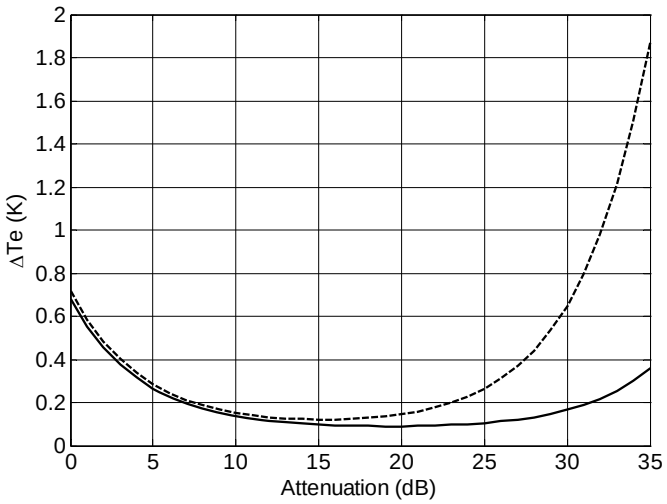

Fig. 3.13. ΔT_e (coverage factor of 3 [3.27]) versus total input path attenuation for two different values of noise source Excess Noise Ratio (ENR): ENR = 20 dB in solid line and ENR = 12 dB in dashed line.

The excess noise ratio of noise sources changes with frequency. In the broadband noise source available in our laboratory, model 346CK01 from Agilent Technologies[1], the ENR ranges from almost 20 dB at 1 GHz to less than 12 dB at 40 GHz. According with Fig. 3.13, the optimum attenuation value is related with the ENR of the noise source. Therefore the best results should be found with a 15 dB attenuator at high frequencies and a 20 dB attenuator at low frequencies.

As well as the receiver uncertainty investigated here to obtain the optimum attenuator insertion loss there are many other error sources that need to be examined in order to make a complete estimation of the measurement uncertainty. These noise sources are investigated in next section, together with the calculation of the total noise measurement uncertainty using Monte Carlo analysis.

3.3. Estimation of Uncertainty in Noise Measurements (based on [3.26])

3.3.1. Introduction

During the measurement process the noise figure meter (NFM) applies the Friis equation (3.18) to obtain the DUT noise since this noise is measured together with the NFM own noise.

$$T_{sys_{meas}} = T_{DUT_{meas}} + \frac{T_{r_{meas}}}{G_{DUT_{meas}}} \rightarrow T_{DUT_{meas}} = T_{sys_{meas}} - \frac{T_{r_{meas}}}{G_{DUT_{meas}}} \tag{3.18}$$

[1] Agilent Technologies, Inc., Santa Clara, CA 95051. USA.

Where the system noise temperature, T_{sys}, is measured at the DUT noise measurement process, and the receiver noise temperature, T_r, is measured at the receiver calibration process. The DUT gain can be obtained from previous measurements.

In the following analysis a general noise measurement configuration is considered, i.e. it can be applied to different setups and measurement techniques, not only the cold-attenuator technique at cryogenics. Furthermore, in order to extent the generality of this analysis different noise sources are considered for the calibration and measurement processes. The configurations for the calibration and measurement are presented in Fig. 3.14.

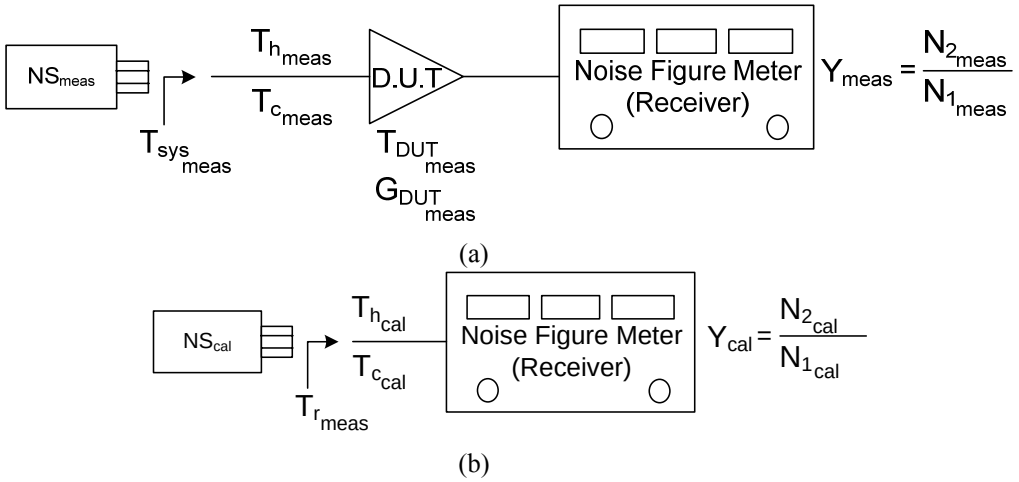

Fig. 3.14. Configurations and definition of variables for the analysis; (a) measurement; (b) calibration.

Where N_i are the measured noise powers in the receiver during calibration and measurement for the two different noise source powers. The calculation of the noise temperatures of the receiver and the system is straightforward using (3.19) and (3.20).

$$T_{sys_{meas}} = \frac{T_{h_{meas}} - Y_{meas} T_{c_{meas}}}{Y_{meas} - 1} \tag{3.19}$$

$$T_{r_{meas}} = \frac{T_{h_{cal}} - Y_{cal} T_{c_{cal}}}{Y_{cal} - 1} \tag{3.20}$$

The received noise powers can be obtained from (3.21)-(3.24).

$$N_{1_{cal}} = kB(T_{c_{cal}} + T_{r_{meas}}) \tag{3.21}$$

$$N_{2_{cal}} = kB(T_{h_{cal}} + T_{r_{meas}}) \tag{3.22}$$

$$N_{1_{meas}} = kBG_{DUT_{meas}}(T_{c_{meas}} + T_{DUT_{meas}} + T_{r_{meas}}) \tag{3.23}$$

$$N_{2_{meas}} = kBG_{DUT_{meas}}(T_{h_{meas}} + T_{DUT_{meas}} + T_{r_{meas}}) \tag{3.24}$$

And finally, the DUT gain is calculated as (3.25).

$$G_{DUT_{meas}} = \frac{N_{2_{meas}} - N_{1_{meas}}}{N_{2_{cal}} - N_{1_{cal}}} \frac{T_{h_{cal}} - T_{c_{cal}}}{T_{h_{meas}} - T_{c_{meas}}} \tag{3.25}$$

In order to calculate the uncertainty in the DUT noise temperature and gain the variables in (3.19), (3.20) and (3.25) are considered to have a random nature. Thus, a large number of measurement iterations can be simulated and the statistics can be extracted from these results. This process is known as Monte Carlo analysis.

To obtain the different noise powers at the receiver it is considered the random nature of all the variables involved in their calculation. As the hot and cold noise temperatures of the calibration and measurement appear both in equations (3.19), (3.20) and (3.25) and in the definition of the received noise powers (3.21) – (3.24), then their random nature is only considered in this last case; otherwise the random behavior will be considered twice and therefore the calculation will be wrong. Therefore the noise temperatures are going to be used as deterministic or random independently, denoting with superscript *r* the random nature.

The deterministic hot and cold temperatures are calculated with (3.26)-(3.29)

$$T_{c_{cal}} = T_{amb} \tag{3.26}$$

$$T_{h_{cal}} = T_{c_{cal}} + T_0 \cdot 10^{\frac{ENR_{cal}(dB)}{10}} \tag{3.27}$$

$$T_{c_{meas}} = \frac{T_{amb}}{L_{attn}} + T_p\left(1 - \frac{1}{L_{attn}}\right) \tag{3.28}$$

$$T_{h_{meas}} = T_{c_{meas}} + T_0 \cdot 10^{\frac{ENR_{meas}(dB) - L_{attn}(dB)}{10}} \tag{3.29}$$

Where T_{amb} is the ambient temperature for the noise source (typically T_{amb} = 296 K), ENR_{cal} is the calibration noise source excess noise ratio, L_{attn} is the total insertion loss of the input path between the noise source and the DUT, ENR_{meas} is the measurement noise source excess noise ratio, and T_p is the physical temperature of the elements in the input path.

In (3.27) and (3.29) the hot temperatures are defined from their cold temperatures, i.e. with the constant difference $T_h - T_c$. This is because the ambient temperature is considered to be different from the standard temperature T_0, and the noise temperatures in both states of the noise source are not independent. The noise generated in the internal attenuator of solid-state noise sources is added to both states [3.22].

3.3.2. Calculation of the received random noise powers

The noise power measured at the receiver with the DUT and the noise source in ON state is given by (3.30), where the Boltzmann's constant and receiver bandwidth are omitted since they are common to all expressions and they do not have a random nature. Subscripts *r* denotes random behavior of the variables.

$$N^r_{2_{meas}} = \Delta G c^r \cdot G^r_{tDUT_{ON}} \left(T^r_{h_{meas}} + T^r_{sys_{ON}} \right) \tag{3.30}$$

The gain in (3.30) refers to *transducer gain*, which is the ratio between the power delivered to a load and the power available from the source. Since it is necessary to obtain the *available gain* to calculate the system noise temperature, then the transducer gain is derived as a function of the available gain (3.31).

$$G^r_{tDUT_{ON}} = G^r_{avDUT_{ON}} \frac{\left(1-\left|\Gamma^r_{out_{ON}}\right|^2\right)\left(1-\left|\Gamma^r_{rec}\right|^2\right)}{\left|1-\Gamma^r_{out_{ON}}\Gamma^r_{rec}\right|^2} \tag{3.31}$$

The different reflection coefficients in (3.31) are defined in Fig. 3.15 and (3.32).

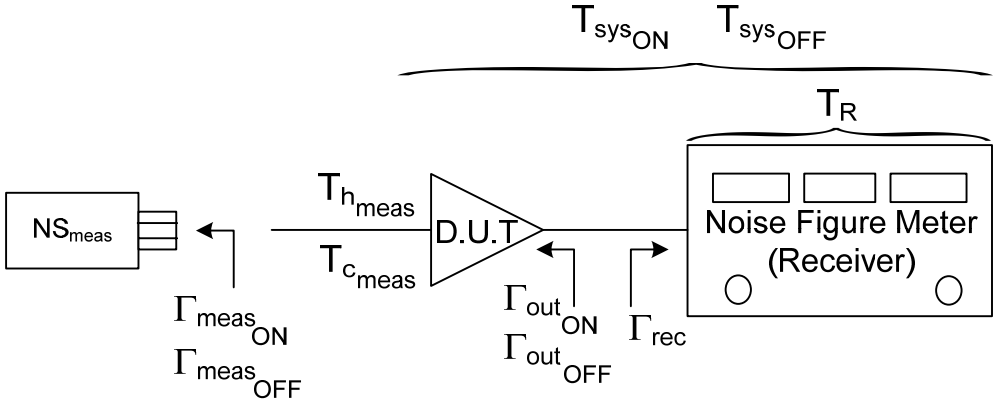

Fig. 3.15. Variables definition for the noise power calculation at DUT measurement.

$$\Gamma^r_{out_{ON}} = S^r_{22} + \frac{S^r_{21}S^r_{12}\Gamma^r_{meas_{ON}}}{1-S^r_{11}\Gamma^r_{meas_{ON}}} \tag{3.32}$$

Where the S_{ij} are the DUT Scattering parameters at the desired frequency. The available gain is given by (3.33).

$$G^r_{avDUT_{ON}} = \frac{\left|S^r_{21}\right|^2\left(1-\left|\Gamma^r_{meas_{ON}}\right|^2\right)}{\left|1-S^r_{11}\cdot\Gamma^r_{meas_{ON}}\right|^2\left(1-\left|\Gamma^r_{out_{ON}}\right|^2\right)} \tag{3.33}$$

On the other hand, the system noise temperature is calculated from Friis formula (3.34).

$$T^r_{sys_{ON}} = T^r_{DUT_{ON}} + \frac{T_R(\Gamma^r_{out_{ON}}, \Gamma^r_{rec})}{G^r_{avDUT_{ON}}} \tag{3.34}$$

In this analysis it is considered that the DUT noise temperature is affected by the noise source reflection coefficient. In order to account for this effect the DUT noise parameters are used to calculate the DUT noise temperature in (3.34) through equations (3.35) and (3.36).

$$T^r_{DUT_{ON}} = T_{\min} + T_0 \frac{g_n}{R^r_g} \left| Z^r_{g_{ON}} - Z_{opt} \right|^2 \tag{3.35}$$

$$Z^r_{g_{ON}} = Z_0 \frac{1 + \Gamma^r_{meas_{ON}}}{1 - \Gamma^r_{meas_{ON}}} \tag{3.36}$$

Where Z_g is the impedance of the noise source, Z_0 is the characteristic impedance, 50 Ω, and T_{min}, g_n, and Z_{opt} are the noise parameters of the DUT.

Finally in (3.34) there is a function, T_R, which is the receiver noise temperature (with an isolator at the input) and it depends on the DUT output reflection coefficient and the receiver input reflection coefficient as given by (3.37) [3.26].

$$T_R(\Gamma_a, \Gamma_b) = T_{rec} + (T_{rec} + T_{iso}) \frac{\left| \Gamma_a - \overline{\Gamma}_b \right|^2}{(1 - |\Gamma_a|^2)(1 - |\Gamma_b|^2)} \tag{3.37}$$

Here, T_{rec} is the minimum receiver noise temperature, i.e. the value measured when the receiver is perfectly matched, and T_{iso} is the physical temperature of the isolator placed at receiver input.

In (3.30) the term ΔG_c was introduced to take into account the uncertainty when the insertion loss of the internal attenuators of the NFM are measured during the calibration process. This information can be found in the NFM manuals as a value expressed in dB, therefore a random variable is generated following a normal distribution (*NORM*) with a mean value of zero and a standard deviation given by the manual (3.38). When this variable is converted from dB to linear scale then it is introduced in (3.30) as a multiplying factor instead of a sum.

$$\Delta Gc^r(dB) = NORM\left(0, \frac{\Delta Gc}{k_{Gc}}\right) \tag{3.38}$$

$$\Delta Gc^r = 10^{\left(\frac{\Delta Gc^r(dB)}{10}\right)} \tag{3.39}$$

The parameters k_i appearing along this analysis are the coverage factors for the random variables and are used to give the expanded uncertainty, i.e. the range where it is believed that the given value is found with a certain probability. Generally a factor of k_i = 1.645 defines an interval with a level of confidence of 90%, a factor of k_i = 2 implies a level of confidence of 95%, and a k_i = 3 defines a confidence greater than 99% [3.27]. Since in the normal distribution the standard deviation value is needed then the uncertainty value given by the equipment manufacturer is divided by its coverage factor, which sometimes is also given by the manufacturer.

Once the mean value of the received noise power has been calculated using (3.30) it is necessary to obtain its uncertainty, which is produced by the limited bandwidth and integration time of the receiver (3.40).

$$\Delta N^r_{2_{meas}} = NORM\left(0, \frac{N^r_{2_{meas}}}{\sqrt{B\tau}}\right) \tag{3.40}$$

Therefore, the new value of the received noise power is given by (3.41).

$$N^r_{2_{meas}} = N^r_{2_{meas}} + \Delta N^r_{2_{meas}} \tag{3.41}$$

Finally, another uncertainty is included in this analysis: the non-linearity of the NFM which may be present between measurements in ON and OFF states. This effect can be included in the analysis as an uncertainty that only is added in the ON state. Once again this data, when available, are given in dB, therefore the normal distribution generated for this effect is added as a multiplying factor in the final noise power (3.42)-(3.44).

$$\Delta G^r_{N^r_{2_{meas}}}(dB) = NORM\left(0, \frac{\Delta G}{k_G}\right) \tag{3.42}$$

$$\Delta G^r_{N^r_{2_{meas}}} = 10^{\left(\frac{\Delta G^r_{N^r_{2_{meas}}}(dB)}{10}\right)} \tag{3.43}$$

$$N^r_{2_{meas}} = N^r_{2_{meas}} \cdot \Delta G^r_{N^r_{2_{meas}}} \tag{3.44}$$

This concludes the calculation of the received noise power with the DUT and the noise source in ON state, including all the considered uncertainties. An analogous process can be followed to obtain the received noise power with the DUT and the noise

source in OFF state, N_{1meas}, just changing ON for OFF in the subscripts and T_h for T_c in the temperatures. The NFM non-linearity uncertainty is not considered in this case.

For the calibration, the calculation of the received noise powers is carried out in a similar way than for the DUT measurement. The are only two differences: the term that includes the uncertainty in the insertion loss measurement of the internal attenuators in the NFM, ΔG_c, is not considered, and the available gain of the DUT is 1. Again, in the calculation of the power with the noise source in ON state, N_{2cal}, is considered the effect of the non-linearity of the receiver, ΔG, which is not included in the calculation with the noise source in OFF state, N_{1cal}. The equations for the calculation with the noise source in ON state are given in (3.45)-(3.51).

$$N^r_{2_{cal}} = G^r_{t_{ON}} \left(T^r_{h_{cal}} + T_R(\Gamma^r_{cal_{ON}}, \Gamma^r_{rec}) \right) \tag{3.45}$$

$$G^r_{t_{ON}} = \frac{\left(1 - \left|\Gamma^r_{cal_{ON}}\right|^2\right)\left(1 - \left|\Gamma^r_{rec}\right|^2\right)}{\left|1 - \Gamma^r_{cal_{ON}} \Gamma^r_{rec}\right|^2} \tag{3.46}$$

$$\Delta N^r_{2_{cal}} = NORM\left(0, \frac{N^r_{2_{cal}}}{\sqrt{B\tau}}\right) \tag{3.47}$$

$$N^r_{2_{cal}} = N^r_{2_{cal}} + \Delta N^r_{2_{cal}} \tag{3.48}$$

$$\Delta G^r_{N^r_{2cal}}(dB) = NORM\left(0, \frac{\Delta G}{k_G}\right) \tag{3.49}$$

$$\Delta G^r_{N^r_{2cal}} = 10^{\left(\frac{\Delta G^r_{N^r_{2cal}}(dB)}{10}\right)} \tag{3.50}$$

$$N^r_{2_{cal}} = N^r_{2_{cal}} \cdot \Delta G^r_{N^r_{2cal}} \tag{3.51}$$

3.3.3. Definition of random variables

Most of the random variables used in the previous sections have not been defined yet and they need to be generated from data obtained from manufacturers or measurements.

All the random variables are considered to follow a normal distribution (*NORM*) or a uniform distribution (*UNIF*); in general, magnitudes will follow the normal distribution whereas phases will follow the uniform distribution in the range (0, 2π).

In order to generate random data following a normal distribution with mean value μ and standard deviation σ it is used the Box-Muller transform (3.52) [3.28].

$$NORM(\mu,\sigma) = \mu + \sigma\sqrt{-2\ln U}\cdot\cos(2\pi V) \tag{3.52}$$

Where U and V are two random values generated following a uniform distribution in the range (0, 1). To generate the data following the uniform distribution in the range (a, b) (3.53) is used.

$$UNIF(a,b) = a + (b-a)U \tag{3.53}$$

In the following, the reflection coefficients are defined as random variables with a magnitude equal to the worst value of the available data and its phase uniformly distributed in (0, 2π).

The reflection coefficient of the calibration noise source in ON state is given by (3.54).

$$\Gamma^r_{cal_{ON}} = \Gamma_{cal_{\max}} e^{-j\phi^r_{cal_{ON}}} \tag{3.54}$$

$$\Gamma_{cal_{\max}} = 10^{\left(\frac{\Gamma_{cal_{\max}}(dB)}{20}\right)} \tag{3.55}$$

$$\phi^r_{cal_{ON}} = UNIF(0,2\pi) \tag{3.56}$$

The noise source reflection coefficients in both states are not independent and hence the coefficient in the OFF state is generated from the one in the ON state through the use of the difference of reflection coefficients (3.57)-(3.59).

$$\Gamma_{cal_{diff}} = 10^{\left(\frac{\Gamma_{cal_{diff}}(dB)}{20}\right)} \tag{3.57}$$

$$\phi^r_{cal_{diff}} = UNIF(0,2\pi) \tag{3.58}$$

$$\Gamma^r_{cal_{OFF}} = \Gamma^r_{cal_{ON}} + \Gamma_{cal_{diff}} e^{-j\phi^r_{cal_{diff}}} \tag{3.59}$$

About the random noise temperatures generated by the noise source they are calculated from the ENR data of the source and the ambient temperature measured by an additional thermometer. Both temperatures, cold and hot, are not considered as independent.

$$T^r_{c_{cal}} = T^r_{amb} \tag{3.60}$$

$$T_{h_{cal}}^{r} = T_{c_{cal}}^{r} + T_0 10^{\frac{ENR_{cal}^{r}(dB)}{10}} \tag{3.61}$$

$$ENR_{cal}^{r}(dB) = NORM\left(ENR_{cal}(dB), \frac{\Delta ENR_{cal}(dB)}{k_{ENR_{cal}}} \right) \tag{3.62}$$

$$T_{amb}^{r} = NORM\left(T_{amb}, \frac{\Delta T_{amb}}{k_{T_{amb}}} \right) \tag{3.63}$$

For the measurement noise source the calculations of the reflection coefficients and noise temperatures are similar to those carried out for the calibration noise source. The only difference is related with the presence of an input path from the noise source to the DUT which is characterized by its insertion loss (including the attenuator or not) and its physical temperature. This difference is accounted for using (3.64)-(3.69).

$$\Gamma_{meas_{diff}} = 10^{\left(\frac{\Gamma_{meas_{diff}}(dB) - 2L_{attn}(dB)}{20} \right)} \tag{3.64}$$

$$T_{c_{meas}}^{r} = \frac{T_{amb}^{r}}{L_{attn}^{r}} + T_p^{r}\left(1 - \frac{1}{L_{attn}^{r}} \right) \tag{3.65}$$

$$L_{attn}^{r} = 10^{\left(\frac{L_{attn}^{r}(dB)}{10} \right)} \tag{3.66}$$

$$L_{attn}^{r}(dB) = NORM\left(L_{attn}(dB), \frac{\Delta L_{attn}(dB)}{k_{L_{attn}}} \right) \tag{3.67}$$

$$T_p^{r} = NORM\left(T_p, \frac{\Delta T_p}{k_{T_P}} \right) \tag{3.68}$$

$$T_{h_{meas}}^{r} = T_{c_{meas}}^{r} + T_0 10^{\frac{ENR_{meas}^{r}(dB) - L_{attn}^{r}(dB)}{10}} \tag{3.69}$$

The input reflection coefficient of the receiver is defined in a similar way than the others.

$$\Gamma_{rec_{\max}} = 10^{\left(\frac{\Gamma_{rec_{\max}}(dB)}{20} \right)} \tag{3.70}$$

$$\phi_{rec}^{r} = UNIF(0, 2\pi) \tag{3.71}$$

$$\Gamma_{rec}^{r} = \Gamma_{rec_{\max}} e^{-j\phi_{rec}^{r}} \tag{3.72}$$

And finally, the S-parameters of the DUT are defined by (3.73)-(3.75).

$$S_{ij}^{r} = S_{ij_{\max}} e^{-j\phi_{S_{ij}}^{r}} \tag{3.73}$$

$$S_{ij_{\max}} = 10^{\left(\frac{S_{ij\max}(dB)}{20}\right)} \tag{3.74}$$

$$\phi_{S_{ij}}^{r} = UNIF(0,2\pi) \tag{3.75}$$

This concludes the mathematical analysis of the noise measurement uncertainty using the Monte Carlo method, which can be adapted to different measurement setups and strategies. Software programs have been developed for these calculations under Matlab and Mathcad platforms [3.24]. These programs can be downloaded from [3.29].

3.3.4. Uncertainty estimation in the cold-attenuator technique

The previous uncertainty analysis is applied in this section to the study of the cold-attenuator technique and the influence of some parameters in the final uncertainty.

The setup for this measurement was presented in Fig. 3.12. The noise source used for receiver calibration is the model N4000A whereas for the DUT measurement the noise source model N4002, both from Agilent Technologies, is used. The reason for using two noise sources with different ENR is to reduce measurement ripples and thus improve its accuracy [3.26]. The input path is comprised of the input coaxial line and the cold-attenuator. The receiver used for this analysis is the NFM model N8975A from Agilent Technologies with an isolator placed at its input in order to improve the receiver matching. Finally, the data from a LNA designed at Centro Astronómico de Yebes, Guadalajara, Spain, for the IF of the band 9 of ALMA project [3.30] are used for the DUT. In Table 3.1 the values of all parameters at the center frequency of 8 GHz used for this analysis are presented.

Parameter	Definition	Value	Unit
	Calibration Noise Source: N4000A		
ENR	Excess noise ratio of the calibration noise source	5.2	dB
ΔENR	Uncertainty of the ENR	0.14	dB
k_{ENR}	Coverage factor of ΔENR	2	
Γ_{max}	Worst value of the source reflection coefficient in ON	-29	dB
Γ_{diff}	Worst value of the difference in coefficients between ON and OFF	-48	dB
T_{amb}	Measured ambient temperature	297	K
ΔT_{amb}	Uncertainty of the ambient temperature thermometer	1	K
k_{Tamb}	Coverage factor of ΔT_{amb}	2	
	Measurement Noise Source: N4002A		
ENR	Excess noise ratio of the measurement noise source	14.1	dB
ΔENR	Uncertainty of the ENR	0.13	dB
k_{ENR}	Coverage factor of ΔENR	2	
Γ_{max}	Worst value of the source reflection coefficient in ON	-24	dB
Γ_{diff}	Worst value of the difference in coefficients between ON and OFF	-24	dB

T_p	Measured physical temperature of the attenuator	12.5	K
ΔT_p	Uncertainty of the attenuator temperature sensor	1	K
k_{Tp}	Coverage factor of ΔT_p	2	
L_{att}	Total attenuation of the input path	15	dB
ΔL_{att}	Uncertainty of the attenuation measurement	0.15	dB
k_{Latt}	Coverage factor of ΔL_{att}	2	
	Receiver: N8975A		
T_{rec}	Minimum noise temperature of the receiver	1500	K
T_{iso}	Measured physical temperature of the isolator	297	K
Γ_{rec_max}	Worst reflection coefficient value at receiver input	-20	dB
B	Receiver bandwidth	4	MHz
τ	Receiver integration time	1	sec
ΔG_c	Uncertainty in internal attenuators insertion loss measurement	0.17	dB
k_{Gc}	Coverage factor of ΔG_c	1.645	
ΔG	Uncertainty produced by receiver non-linearity	0.05	dB
k_G	Coverage factor of ΔG	1.645	
	DUT: LNA 4 – 12 GHz Band 9 of ALMA		
S_{11}	Input reflection coefficient	-3.5	dB
S_{21}	Transmission coefficient	33.5	dB
S_{12}	Reverse transmission coefficient	-47	dB
S_{22}	Output reflection coefficient	-13	dB
T_{min}	Minimum noise temperature (noise parameter)	3.74	K
g_n	Noise parameter	6.74e-5	S
$Re(Z_{opt})$	Real part of optimum noise impedance (noise parameter)	77.9	Ω
$Im(Z_{opt})$	Imaginary part of optimum noise impedance (noise parameter)	71.1	Ω
	Monte Carlo Parameters		
Iterations	Number of iterations in the Monte Carlo analysis	10000	
k	Coverage factor for the Monte Carlo results	2	

Table 3.1. Data for the Monte Carlo analysis in the cold-attenuator technique.

For this DUT it is expected a nominal gain of 33.5 dB and a nominal noise temperature of 6 K at the frequency of 8 GHz when cooled down to 12.5 K. With the parameters shown in Table 3.1 the Monte Carlo analysis gives the following results extracted from the developed program with a coverage factor of 2.

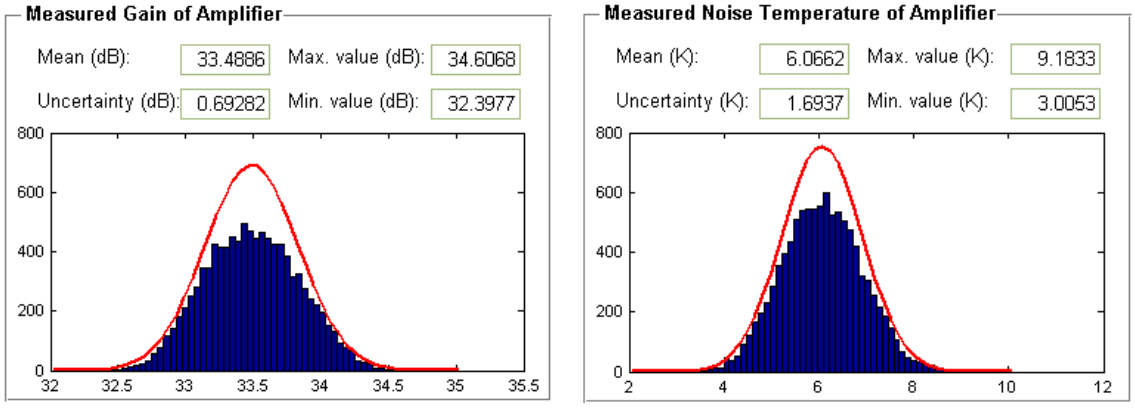

(a) (b)

Fig. 3.16. Results of the Monte Carlo analysis for the ALMA LNA using the cold-attenuator technique; (a) gain results; (b) effective input noise temperature results.

Therefore, a total uncertainty of around 1.7 K in the noise temperature for the presented setup is found. This value agrees well with other studies made with other DUTs, setups and mathematical approaches [3.31].

Taking advantage of the developed program it is easy to vary some parameter values in order to check the change of the total uncertainty, thus extracting conclusions that may help during the measurement process. Some plots are presented in the following figure to show these variations.

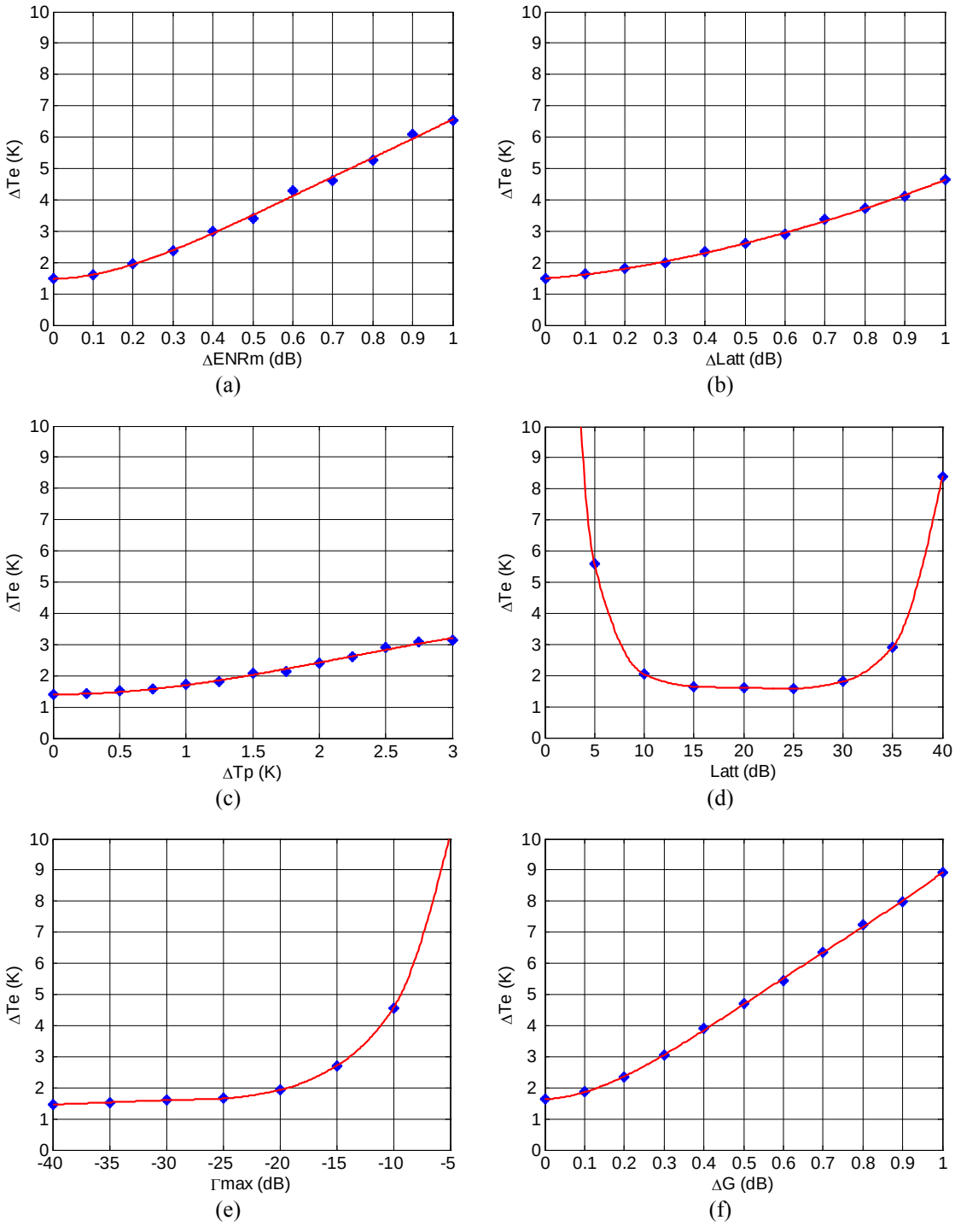

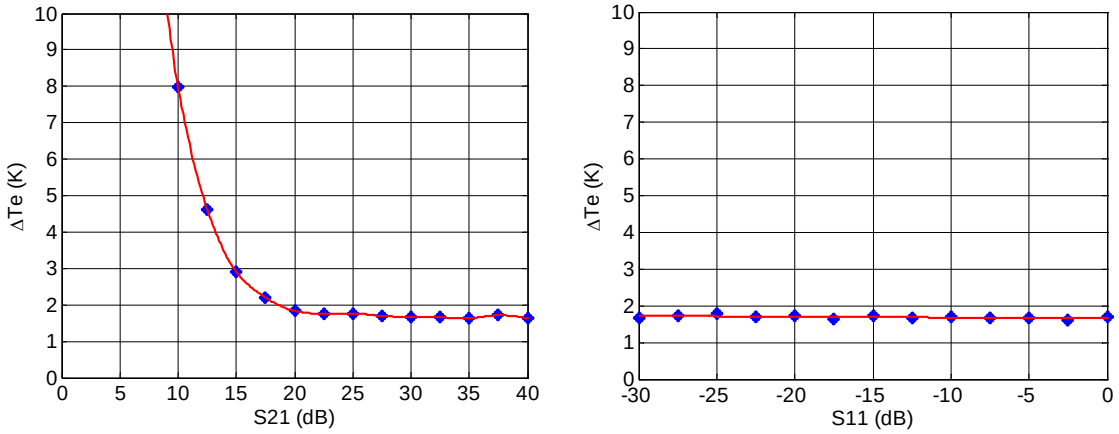

Fig. 3.17. Effect of the variation of some parameters of the Monte Carlo analysis on the noise temperature uncertainty; (a) uncertainty of measurement noise source ENR; (b) uncertainty of the measurement of input path insertion loss; (c) uncertainty of physical temperature of the cold-attenuator; (d) value of the input path insertion loss; (e) value of the measurement noise source reflection coefficient; (f) uncertainty in receiver non-linearity; (g) DUT gain value; (h) DUT input reflection coefficient value.

From Fig. 3.17 some conclusions can be extracted:

- The uncertainty of the measurement noise source greatly affects the final measurement uncertainty; hence calibrated noise sources are important for accurate results.
- The input path needs to be accurately characterized both in insertion loss and physical temperature.
- As demonstrated in Section 3.2.2.5 with a simpler mathematical approach, there is an optimum value for the input path insertion loss which depends on the setup.
- The reflection coefficient of the measurement noise source can ruin the measurement accuracy; therefore high quality noise sources are advisable.
- The receiver linearity affects linearly the measurement uncertainty, however this value is given by the available receiver and nothing can be done to reduce this value but to try to work in the linear range.
- Low gain DUTs can not be measured with this setup since the DUT gain has to be large enough to overcome the high insertion losses of the setup, thus enabling the receiver to measure suitable signals.
- The DUT input reflection coefficient has no effect with this setup since the attenuator provides a good matching between the noise source and the DUT.

3.4. Chip Attenuator for Improving Noise Measurement Accuracy

3.4.1. Introduction

In order to take precise T_e measurements using the cold-attenuator technique, the physical temperature of the attenuator must be precisely known. Moreover, in most cases, the uncertainty in the temperature of the sensor calibration is the greatest error

source in the measurement [3.24], [3.26], [3.31], [3.32]. For thermal characterization, a temperature sensor is attached to the attenuator body. The problem arises when using coaxial attenuators since the temperature of the inner conductor, where the resistive elements are placed, cannot be directly measured. This is relevant since the temperature of these resistive elements is often raised due to the heat transferred through the inner conductor of the coaxial cable connecting to the ambient port of the cryostat.

If the sensor reading is used directly for the calculations T_e will be overestimated by approximately the same amount as the difference in physical temperature. One option to avoid this is to correct the reading of the physical temperature with an offset determined by a calibration performed by noise measurements of a known device. Other possible option is to insert an additional element in the input line to provide some thermal isolation of the inner conductor of the coaxial line as in [3.33]. In the first case the error in the measurement would have a magnitude close to the accuracy of the calibration performed; while in the second case, the additional element introduces more uncertainty in the measurement of the insertion loss of the input line, increases the ripple of the transmission and deteriorates the reflection.

The approach presented in this thesis is to use an attenuator with a much better cryogenic thermal link to its body to avoid the drawbacks of the previous approaches. This improved thermal link is accomplished through the use of a high thermal conductivity substrate and high thermal stability thin film resistors in the attenuator chip design, thus avoiding the resistors heating through the inner conductor. Two versions of the chip attenuator were designed, one with 15 dB and the other one with 20 dB insertion loss (optimum insertion losses according with Section 3.2.2.5). This thesis only presents the design process and results of the 20 dB unit for clarity.

3.4.2. Attenuator chip design

The 20 dB attenuation is accomplished by cascading four basic T-network [3.34], [3.35] cells of 5 dB attenuation each one. Therefore, the electrical design process is simplified to the design of one basic cell. If only one cell is implemented to achieve the 20 dB attenuation then the parasitic capacitance to ground of the large series resistors would reduce the chip bandwidth. Figure 3.18 shows the schematic of this cell with the resistive elements forming a T-network. The shunt element in this configuration is divided into two parallel resistors to maintain symmetry in the structure and to reduce the inductance to ground.

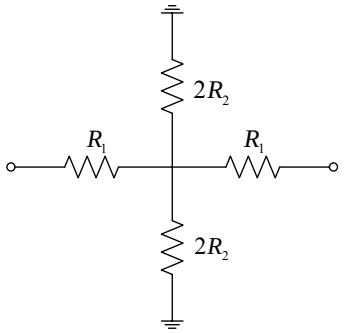

Fig. 3.18. T-network basic cell.

Values for resistors R_1 and R_2 can be found applying equations (3.76) and (3.77) [3.34], [3.35].

$$R_1 = Z_0 \frac{1 - S_{21}}{1 + S_{21}} \tag{3.76}$$

$$R_2 = 2 \cdot Z_0 \frac{S_{21}}{1 - S_{21}^2} \tag{3.77}$$

Where Z_0 is the characteristic impedance, 50 Ω, and S_{21} the desired insertion loss (linear). For 5 dB attenuation, R_1 = 14 Ω and R_2 = 82.2 Ω.

One of the key aspects in the chip design is the substrate selection. To minimize the temperature difference between the resistive elements in the chip and the attenuator body, a substrate with high thermal conductivity at cryogenic temperatures is needed. The attenuator has been designed using thin film technology from ATC[2]. Crystal quartz, CQ, (z-cut, ε_r = 4.44 and h = 5 mils) has been the selected substrate since it shows a high thermal conductivity of 1000 W/mK at 10 K [3.36]. For comparison, Teflon has a thermal conductivity of 0.1 W/mK at 10 K [3.37] and Alumina has a thermal conductivity of 7 W/mK at 10 K [3.36], [3.38].

For the resistors, a nickel chromium (NiCr) thin film is preferred due to its low resistivity variation with temperature, but only tantalum nitride (TaN) resistors were available for ATC process with this substrate. However, TaN resistors also show a low temperature coefficient of resistance, TCR, of -50 to -100 ppm/ºC in the -25 ºC to 125 ºC temperature range (0 to 50 ppm/ºC for NiCr resistors) which make them suitable for large temperature gradients. In order to check the low TCR of TaN resistors at cryogenics some DC measurements have been carried out once the attenuator was finished. These results are presented in Section 3.4.4. Electrical performance of the attenuator depends on the resistors accuracy; therefore resistors were designed with -

[2] American Technical Ceramics Thin Film Technologies, Jacksonville, FL 32216. USA.

20% resistance values for laser trimming, with 1% tolerance, during chip processing. Individual via holes enable to trim each resistor individually before via holes thru plating.

Two versions of the 20 dB attenuator were designed, one with microstrip ports, for being mounted in the attenuator module with coaxial connectors, and other with coplanar-to-microstrip transitions to perform RT chip tests in a coplanar probe station. The layout of the latter is shown in Fig. 3.19.

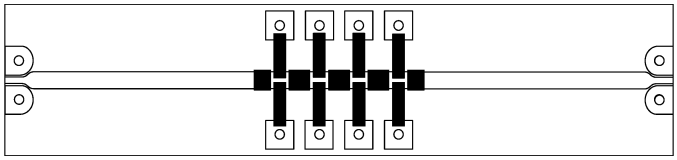

Fig. 3.19. Chip layout of the 20dB attenuator. Resistors are 20% larger and via holes are independent for laser trimming. Coplanar-to-microstrip transitions designed for testing in a probe station. Dimensions are 9x2 mm^2.

The attenuator was designed using Microwave Office from AWR[3] both for schematic optimization and electromagnetic verification. Electromagnetic simulation results of the 20 dB chip with full length microstrip accesses and without coplanar-to-microstrip transitions are presented in Figs. 3.20 and 3.21, together with on-wafer measurement results taken in a coplanar probe station at RT.

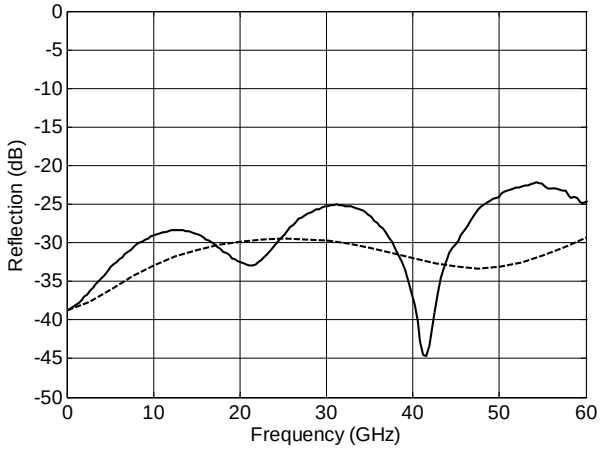

Fig. 3.20. Simulated (dashed line) and measured (solid line) reflection of the 20 dB attenuation chip at RT. Measurement includes coplanar-to-microstrip transitions, which are not taken into account in simulation.

[3] AWR Corp., El Segundo, CA 90245. USA.

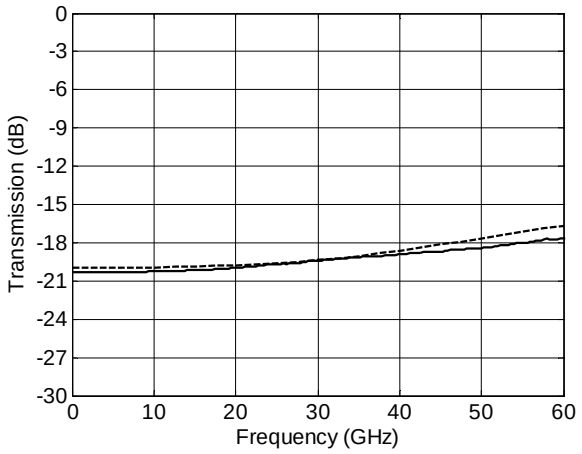

Fig. 3.21. Simulated (dashed line) and measured (solid line) transmission of the 20 dB attenuation chip at RT. Measurement includes coplanar-to-microstrip transitions, which are not taken into account in simulation.

On-wafer chip measurements show an insertion loss of 19.55 dB ± 0.75 dB in the DC to 40 GHz range with a return loss better than 25 dB. These measurements also demonstrate that this chip can be used at higher frequencies if needed, designing a suitable assembly.

3.4.3. Attenuator module assembly

The attenuator is intended to be used up to 40 GHz therefore the module is designed accordingly. The module has been machined in brass (thermal conductivity of 10 W/mK at 10 K [3.39]) using a numerically controlled milling machine and then nickel and gold-plated to avoid oxidation and to provide a solderable surface.

A temperature sensor model DT-670 from LakeShore[4] with an uncertainty of ±0.25 K has been soldered close to the chip location as shown in Fig. 3.22. The proximity between the sensor and the attenuator chip, and especially the high thermal conductivity of brass, gold and crystal quartz, makes the temperature gradient negligible between them, minimizing the uncertainty in the determination of the attenuator temperature. Sensor terminals are directly soldered to a hermetic DC header to provide current bias and voltage measurement. The attenuator chip is attached to the module using Indalloy290[5] (97% In, 3% Ag) paste which produces a soft joint between parts and avoids cracks during thermal cycles. Due to its high indium content, Indalloy290 takes advantage of indium ductility [3.40] and high thermal conductance [3.41] at cryogenic temperatures. Moreover, indium-based solders produce less scavenging damage than regular tin-based solders for use on gold films; therefore the formation of brittle intermetallic layers is minimized.

[4] Lake Shore Cryotronics, Inc., Westerville, OH 43082-8888, USA.

[5] Indium Corporation of America, Utica, NY 13502. USA.

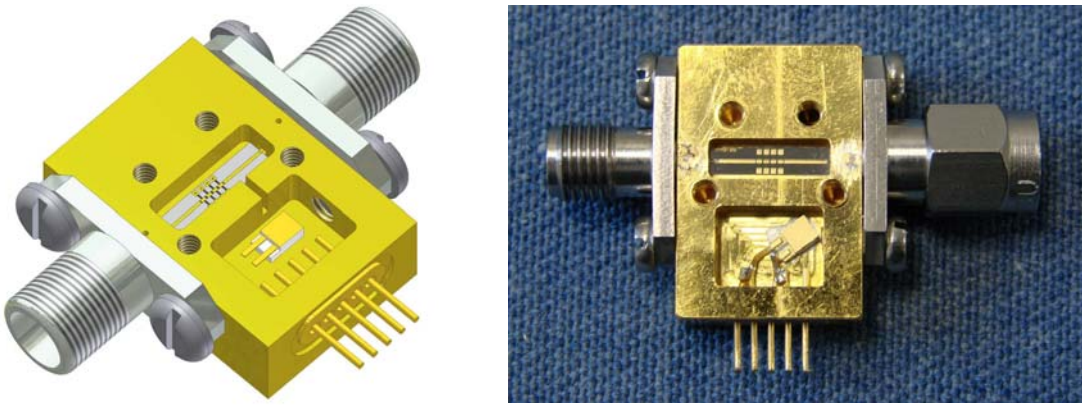

(a) (b)

Fig. 3.22. Attenuator module with cover removed; (a) design and (b) final assembly. Dimensions are 20.5x13.6x7.7 mm^3, excluding connectors.

The module is fitted with K-connectors (2.92 mm). The low temperatures produce the contraction of the materials. Since the coefficients of thermal expansion (CTE) are different for the different parts, cracks may be produced in the joints; therefore sliding contacts are installed in the glass bead pins of the connectors. These sliding contacts are soldered with regular SnPb solder to the microstrip line but they are free to move along glass bead pin minimizing problems produced by thermal stress. Finally, two holes are drilled in one side in order to thermally anchor the module to the cold plate in the cryostat.

3.4.4. Attenuator module characterization

Attenuator characterization has been carried out at room temperature while additional measurements at cryogenic temperature have been taken in order to obtain performance variations upon cooling.

At room temperature, measurements have been made using PNA E8364C from Agilent Technologies together with short, open, load and thru standards (SOLT calibration). Results obtained with these measurements are presented by solid lines in Figs. 3.23 and 3.24. These results show return losses better than 20.6 dB (VSWR of 1.20) and insertion losses of 19.9 dB ± 0.65 dB in the DC to 40 GHz frequency range.

At cryogenic temperature a precise S-parameters measurement is quite difficult to obtain due to direct inaccessibility to DUT ports, which complicates a proper system calibration. Cryogenic measurements have been carried out using the existing setup at Centro Astronómico de Yebes, CAY, Guadalajara, Spain. For the cryogenic S-parameters measurement, the reference plane is set inside the cryostat, at the point of the connection of the DUT. The calibration is performed at room temperature using an electronic calibration kit (ECAL) from Agilent Technologies connected at the same position as the DUT. After that, cryogenic measurements of two shorts and one thru standards are taken in different cool-downs and used to make the small corrections

needed in the previous calibration for accurate cryogenic measurements. Moreover, time domain gating is used to eliminate the small variations in reflection produced in the input and output cryostat transitions when cooled. This measurement is limited to 20 GHz due to limited bandwidth of electro-mechanic switches installed in the existing setup. Cryogenic reflection results, presented in Fig. 3.23 with a dashed line, are further limited to 18 GHz to avoid non consistent results produced at band edges by the time domain gating. These results show small reflection variation upon cooling in the measured range, which is expected to be maintained up to 40 GHz.

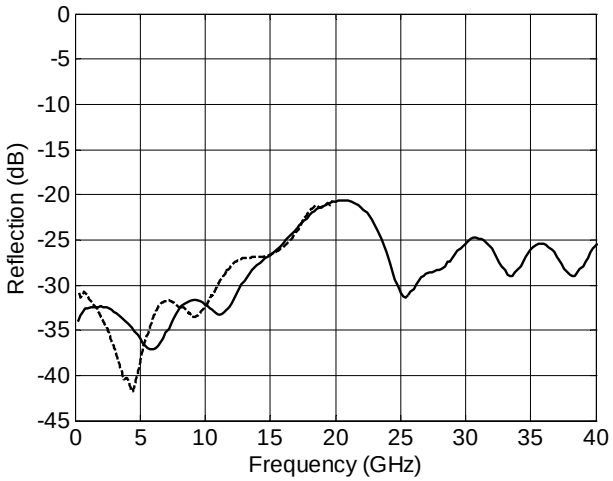

Fig. 3.23. Measured reflection, S_{11}, of attenuator module at room temperature in solid line and at cryogenic temperature (T = 15 K) up to 18 GHz in dashed line.

The attenuation at cryogenic temperature should be characterized up to 40 GHz since its value is a key factor for obtaining meaningful noise measurements with the cold-attenuator technique. As the previously described system did not allow measurements over 18 GHz another strategy was chosen. A different cryostat with K (2.92 mm) connectors and stainless steel transitions was used. First, the input and output coaxial lines in the cryostat were measured in a back-to-back configuration both at room and cryogenic temperatures. From these measurements the change in the coaxial lines' insertion losses as a function of frequency was measured and modeled. Then, the attenuator was inserted between the coaxial lines and the overall insertion loss of all elements was measured both at room and cryogenic temperatures. Finally the effect of the coaxial lines was subtracted and the insertion loss of the attenuator was obtained at both temperatures. These results were used to model the variation of the attenuation with temperature since the measurements inside of the cryostat are affected by ripples produced by reflections in the input lines. From the previous results, it was determined that a simple correction factor of the form given by (3.78) could be used to model the reduction of loss experienced when cooling either the input lines or the attenuator. This correction factor is applied to the room temperature attenuation measurement, taken outside of the cryostat using SOLT calibration and depicted with solid line in Fig. 3.24,

obtaining a model of the insertion loss at 15 K, which is plotted with dashed line in Fig. 3.24.

$$C(dB) = A \cdot f(GHz)^{1/B} \cdot \frac{T_2 - T}{T_2 - T_1} \tag{3.78}$$

The formula assumes a linear variation of the losses with temperature. The constant A is 0.0384 for the stainless steel coaxial lines of the available setup and 0.0079 for the attenuator, whereas B is 1.563 for the coaxial lines and 1 for the attenuator. Equation (3.78) is linearly scaled for any temperature T between T_2 = 295 K and T_1 = 15 K.

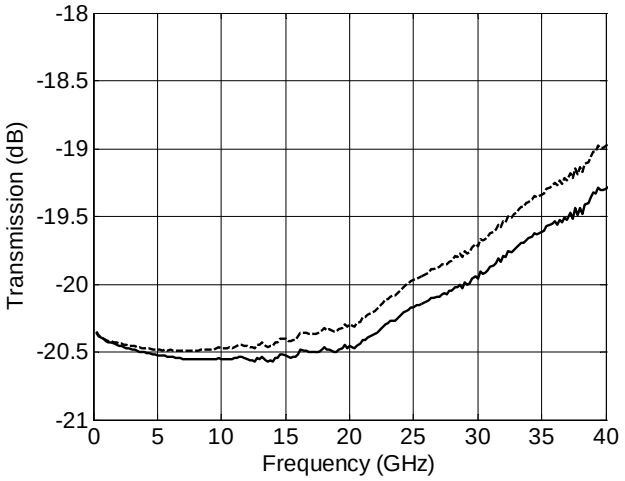

Fig. 3.24. Measured transmission, S_{21}, of attenuator module at room temperature (solid line) and modeled transmission at cryogenic temperature (T = 15 K) (dashed line). The modeled values are obtained applying the correction factor given by (3.78) to the room temperature measurement.

From the attenuation change extracted model, an increasing reduction of the attenuator insertion loss with frequency is clearly seen. This effect is explained with the improvement of electrical conductivity of gold in the microstrip lines and connectors upon cooling. In order to prove this assumption an electromagnetic simulation of the attenuator chip, i.e. excluding connectors, was performed in HFSS[6] varying the electrical conductivity of gold and the results, presented in Fig. 3.25, were found similar to those shown in Fig. 3.24. The value of the electrical conductivity of gold at cryogenic temperature was increased in an order of magnitude from its room temperature value [3.42].

[6] Ansoft, LLC. Pittsburgh, PA 15219. USA.

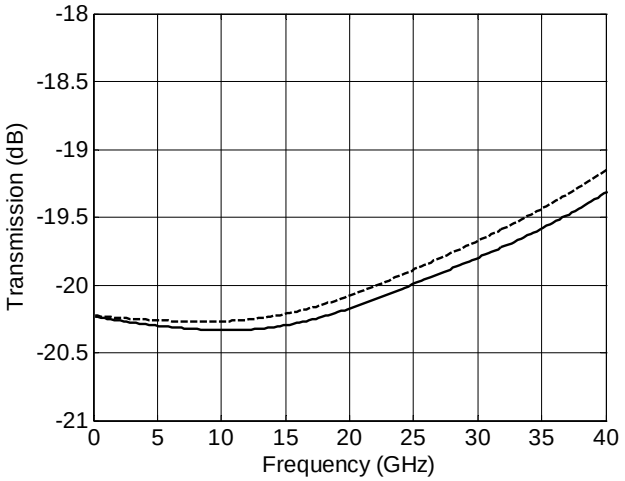

Fig. 3.25. HFSS simulation of chip attenuator insertion loss at room temperature (solid line) and at cryogenic temperature (dashed line). The electrical conductivity of gold at cryogenics has been increased an order of magnitude from its room temperature value [3.42].

Finally, the thermal stability of TaN resistors has been investigated with DC measurements. The DC resistance at one port of the attenuator with the other port open was carefully measured correcting for the change of resistance of the connecting cables when cooling. This measurement has shown an increase of DC resistivity in the chip of 2% at 15 K, i.e. a TCR of -70 ppm/K, practically constant in the 15 K to 290 K temperature range, which confirms the good thermal stability of TaN resistors at cryogenic temperature. This small variation has a very small effect in the change of the loss and match of the attenuator. The simulation of the attenuator with this small DC resistivity increment shows a negligible change of the insertion loss (bellow 0.03 dB) and a variation of the return loss less than 2 dB at the worst matched frequency point. The dominant effect in the observed variation of the loss is the change of the connecting microstrip lines.

3.4.5. Low noise amplifier noise measurement

To demonstrate the performance of the designed attenuator a well-known LNA is measured both with the new attenuator and with the classical noise setup available at CAY, taking into account the loss variation extracted in the previous section. The selected DUT is a prototype of the same LNA used in Section 3.3.2 [3.30]. The classical noise setup uses cascaded 6 dB and 10 dB commercial coaxial attenuators up to 40 GHz. In these attenuators, the outer conductor, where the temperature sensor is attached, is directly connected to the cold plate and it is probably colder than the inner conductor, which is heated through the coaxial lines. At the CAY this problem is reduced using a home-made heat-block before the first coaxial attenuator. This heat-block is comprised of a series of two K-female sparkplug launcher transitions interconnected by a glass bead so the contact makes a relatively high thermal resistance connection at cryogenic

temperature [3.33]. The noise measurement result[7] obtained with this classical setup is plotted in solid line in Fig. 3.26. For the measurement with the new attenuator, both the coaxial attenuators and the heat-block are replaced by the new attenuator module. The result of this new measurement is shown in dashed line in Fig. 3.26.

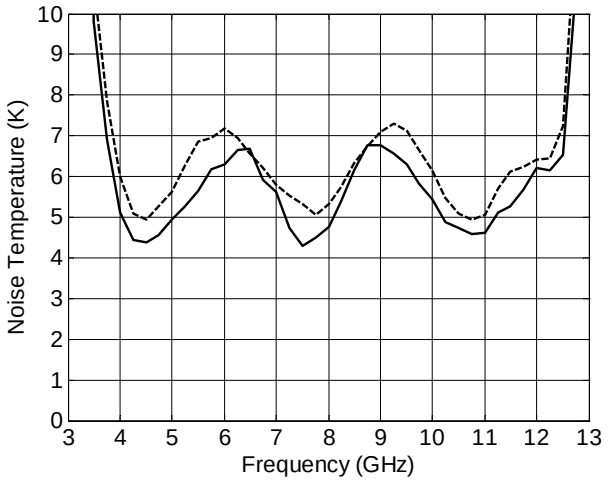

Fig. 3.26. Noise temperature measurement of the ALMA prototype LNA at cryogenic temperature. Measurement result with commercial attenuators (10 + 6 dB) plus a home-made heat-block is shown in solid line whereas measurement result with the new attenuator is plotted with dashed line. (Ripples are inherent to the amplifier).

Figure 3.26 shows similar results for both setups. The same sensor (model DT-470 from LakeShore), attached to the attenuators body, was used in both measurements in order to eliminate its influence in noise results due to different calibrations. The small differences between the setups with heat-block and with the designed attenuator shown in Fig. 3.26 demonstrate that this new design does not suffer from appreciable heating through the input lines. Using the analysis developed in Section 3.3, the total uncertainty of this measurement at 8 GHz is ±1.7 K considering sensor DT-470 (uncertainty ±1 K). This total uncertainty can be lowered to ±1.3 K if the temperature value from sensor DT-670 (uncertainty ±0.25 K) is used. This total uncertainty is defined with a coverage factor of 2, which means a 95.45% confidence.

3.5. Conclusions

In this chapter an overview of different techniques used for S-parameters and noise measurements in a cryogenic environment is given. About the S-parameters measurement, this chapter focuses in a calibration technique that improves the measurement accuracy when drift errors are present and demonstrates its reliability with a simple test, where one transistor is measured both with the classical TRL calibration technique and with the proposed procedure.

[7] Note that ripples in the noise plot are intrinsic to the amplifier, which is a prototype designed to test the effect of a long input matching line.

Among the presented noise measurement techniques in cryogenics, the cold-attenuator technique is detailed with an analysis where the optimum value for the attenuator insertion loss is carried out. This technique is complemented with a comprehensive study of the uncertainty in the noise measurement using the Monte Carlo analysis. Finally, the design and characterization of an attenuator to improve the noise measurement accuracy is shown. This attenuator is based on a chip designed in a high thermal conductivity substrate with high thermal stability thin film resistors achieving negligible temperature gradient between the chip and the temperature sensor, thus improving the measurement accuracy.